Dynamic thermal-hydraulic modelling of the EU DEMO HCPB breeding blanket cooling loops

Dynamic thermal-hydraulic modelling of the EU DEMO HCPB breeding blanket cooling loops

A. Froio[a], C. Bachmann[b], F. Cismondi[b], L. Savoldi[a] and R. Zanino[a,] *

[a] *NEMO group, Dipartimento Energia, Politecnico di Torino, 10129 Torino, Italy*
[b] *PPPT Department, EUROfusion Consortium, 85748 Garching bei München, Germany*

* *Corresponding author:* roberto.zanino@polito.it

Abstract

A global, system-level thermal-hydraulic model of the EU DEMO tokamak fusion reactor is currently under development and implementation in a suitable software at Politecnico di Torino, including the relevant heat transfer and fluid dynamics phenomena, which affect the performance of the different cooling circuits and components and their integration in a consistent design. The model is based on an object-oriented approach using the Modelica language, which easily allows to preserve the high modularity required at this stage of the design. The first module of the global model will simulate the blanket cooling system and will be able to investigate different coolant options and different cooling schemes, to be adapted to the different blanket systems currently under development in the Breeding Blanket (BB) project. The paper presents the Helium-Cooled Pebble Bed (HCPB) module of the EU DEMO blanket cooling loops system model. The model is used to compare different schemes for the cooling of the different components of the HCPB BB, and to suggest improvements aimed at optimizing the pumping power required by the cooling system. The model is then used to analyse a pulsed scenario, characteristic of the EU DEMO operation.

Keywords

Nuclear fusion, DEMO, breeding blanket, HCPB, cooling circuit, thermal-hydraulics, modelling

Nomenclature		Unit
A	Area of channel cross section	m²
c_v	Specific heat at constant volume	J/(kg K)
D_h	Hydraulic diameter	m
e	Specific energy	J/kg
f	Fanning friction factor	-
h	Specific enthalpy	J/kg
K	Localized pressure loss coefficient	-
l	Length	m
$\dot{m}$, dm/dt	Mass flow rate	kg/s
Nu	Nusselt number	-
p	Pressure	Pa
Δp	Pressure drop	Pa
Pr	Prandtl number	-
$\dot{Q}$	Heat load	W
Re	Reynolds number	-
T	Temperature	K
t	Time	s
V	Volume	m³
v	Velocity	m/s
Greek		
γ	Heat transfer coefficient	W/(m² K)
ρ	Density	kg/m³
Subscripts		
i	Volume index	
m	Metal structures	
in	Inlet	
out	Outlet	
Abbreviations		
Acronyms		
BB	Breeding Blanket	
BC	Boundary Condition	
BM	Breeding Module	
BSS	Back Supporting Structure	
BZ	Breeding Zone	
CAD	Computer-Aided Design	
CFD	Computational Fluid Dynamics	
CP	Cooling Plate	
DIV	Divertor	
EU DEMO	European Demonstration Fusion Power Reactor	
FV	Finite Volume	
FW	First Wall	
HCPB	Helium-Cooled Pebble Bed	
HCPB-D	HCPB-Detached	
HCPB-I	HCPB-Integrated	
HCPB-S	HCPB-Separated	

HIP	Hot Isostatic Pressing
HTC	Heat Transfer Coefficient
HX	Heat eXchanger
IB	Inboard
OB	Outboard
OOP	Object-oriented programming
PHTS	Primary Heat Transfer System
PMU	Project Management Unit
SG	Steam Generator
TBM	Test Blanket Module
WCLL	Water-Cooled Lithium Lead
WPBB	Work Package Breeding Blanket

1. Introduction

Within the framework of the Horizon 2020 EU fusion roadmap [1], the conceptual design of a European Demonstration Fusion Power Reactor (EU DEMO) is under development. After ITER, this device shall demonstrate the operation in a closed fuel cycle (i.e. tritium self-sufficiency) and the production of net electricity. The development of a global thermal-hydraulic model of the EU DEMO tokamak has been launched by the EUROfusion Project Management Unit (PMU) to simulate the cooling loops of the main in-vessel components, including the ex-tokamak parts. The model shall be based on an object-oriented approach, in order to be sufficiently modular to follow-up the design development.

The development of this model, which will be the first system-level thermal-hydraulic model to be developed for the power cycle of DEMO, has started in 2015 in the Energy Department at Politecnico di Torino. Up to now, engineering modelling efforts for DEMO mainly focused on other kind of system-level analyses (e.g. global thermal analysis [2]), or on component-level CFD analyses, see e.g. [3]. For ITER, some system-level analyses have been carried on for the BB cooling system and related to safety studies for the EU [4], Korean [5] and Chinese [6] Test Blanket Modules (TBMs), as well as analyses of the thermal-hydraulics of other systems (e.g. the superconducting magnet system, [7]); also for ITER, of course, extensive component-level CFD analyses were performed [8, 9].

The first module of the global model will allow the transient simulation of the BB cooling system, which has to remove ~80% of the total thermal power produced in the reactor and to integrate it into a power generation system. This model shall be able to investigate different coolant options and different cooling schemes, in order to simulate the different blanket systems currently under development in the EUROfusion Breeding Blanket Work Package (WPBB), determining the resulting thermal-hydraulic and thermodynamic performances, depending on different heat load distributions on the plasma facing components.

In this paper we present the development and first application of a version of the first module of the code, devoted to the Helium-Cooled Pebble Bed (HCPB) BB concept. Another version, devoted to the Water-Cooled Lithium Lead BB concept, is currently under development.

2. The HCPB cooling circuit

For the development of this model, the 2014 design of the HCPB BB [10], which is shortly described in the following, has been considered; anyway, thanks to the modular approach used, the model can be easily adapted to any successive design.

The EU DEMO 2014 design foresees 16 toroidal sectors (22.5° each), each sector being made of three Outboard (OB) and two Inboard (IB) blanket segments, see Figure 1, for a total of 48 OB and 32 IB segments; all the OB segments are equal, as well as all the IB segments. Each segment contains 6 Breeding Modules (BMs), see Figure 2.

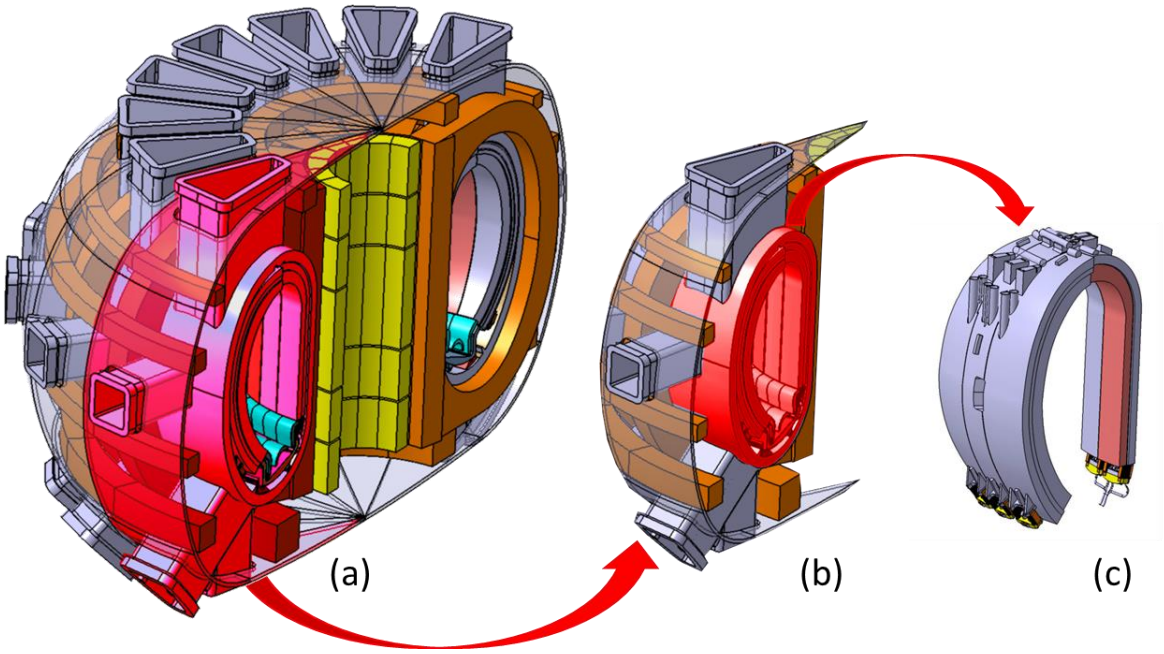

Figure 1: (a) Sketch of half of the 2014 EU DEMO tokamak, divided in 8 sectors; (b) single sector, (c) 5 blanket segments, three outboard and two inboard, constituting the single sector. Adapted from [11].

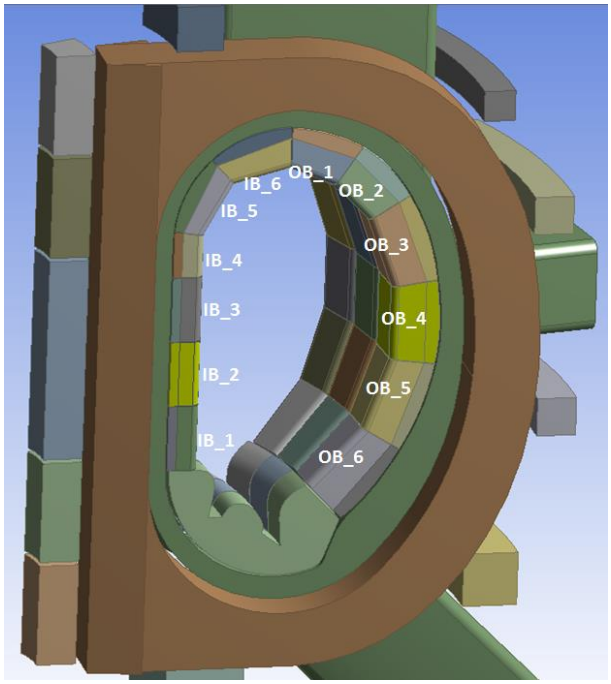

Figure 2: A 2014 EU DEMO sector, showing the numbering of the Breeding Modules; the numbering is equal for all the segments [12].

A CAD snapshot of the HCPB OB4 BM is shown in Figure 3a. On the outer part, facing the inner shell of the Vacuum Vessel, the Back Supporting Structure (BSS) contains the coaxial inlet and outlet manifolds. The Breeding Zone (BZ) is a vertical stack of horizontal cooling plates (CPs, 5 mm thick) alternated with Li_4SiO_4 pebble bed (breeder, 11 mm thick) and Be pebble bed (neutron multiplier, 33 mm thick) [13], see Figure 3b. The BZ is enclosed between two caps above and below, and is limited by the first wall (FW) on the plasma facing side, as well as on the two lateral sides.

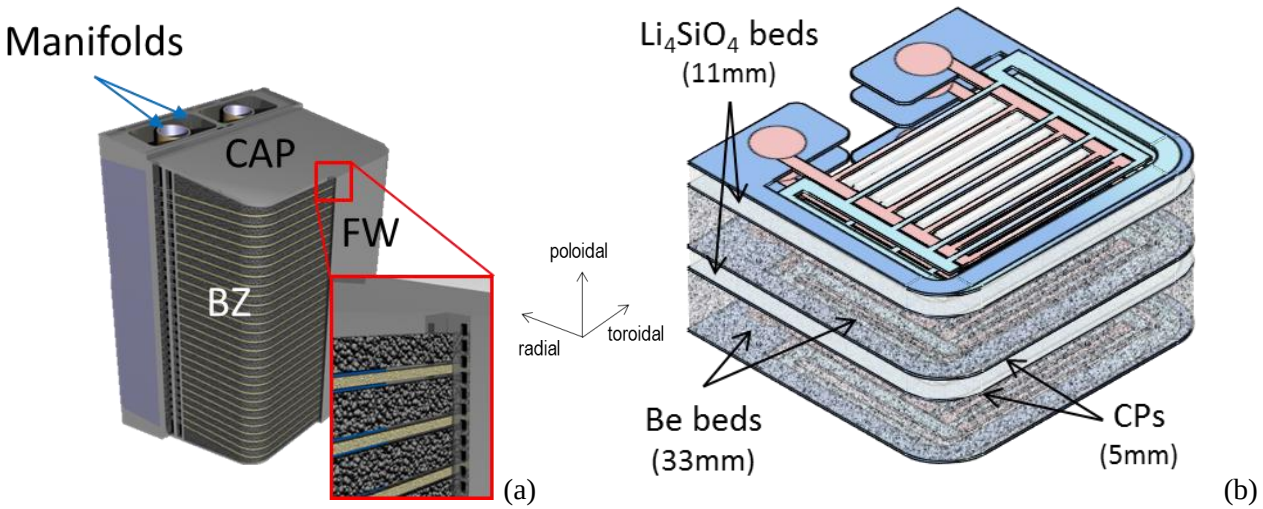

Figure 3: a) CAD drawing of the OB4 BM, showing the detail of the FW and BZ in the inset; b) detail of the BZ: the thickness of the different layers is reported in the brackets. Adapted from [13].

The FW is heated by a surface load from the plasma on its front part, and by a volumetric nuclear load; moreover, ~8% of the heat generated in the BZ (i.e., heat produced by exothermic nuclear reactions and decay heat) is conducted to the FW [12]. The FW is cooled by pressurized helium flowing inside square channels, see Figure 3a, which are in a different number for each BM depending on the poloidal location of the module, see Table 1; similarly, the number of CPs varies with the BM location, as reported in Table 1. Each CP is a Hot Isostatic Pressed (HIPed) plate with 36 parallel rectangular cooling channels, see Figure 4, that have to remove ~92% of the heat generated in the BZ, as well as the heat produced by the nuclear load. The caps are HIPed plates with 22 parallel rectangular cooling channels; the CPs and caps cooling channels are unevenly distributed in the radial direction, see the inset in Figure 4, as the distance between two channels becomes smaller approaching the plasma-facing wall. Also, the channels closer to the plasma are slightly shorter, because of the shape of the BM.

Table 1: Number of FW channels and cooling plates per BM.

		BM1	BM2	BM3	BM4	BM5	BM6
FW channels	Inboard modules	104	104	103	85	80	80
	Outboard modules	97	106	106	112	112	112
Cooling plates	Inboard modules	63	63	63	40	55	53
	Outboard modules	45	49	71	71	71	73

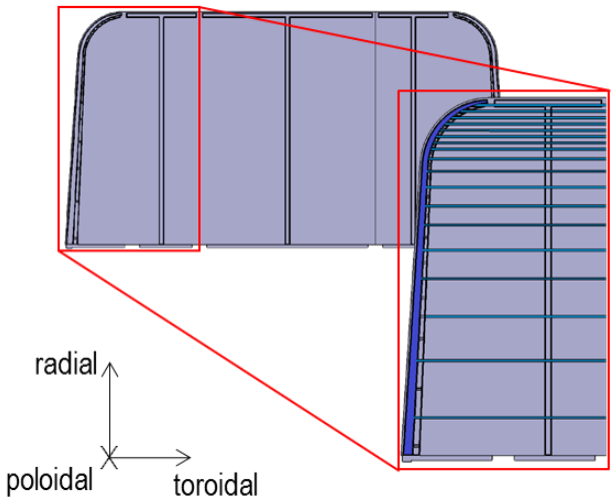

Figure 4: CAD of a CP, showing a manifold and the 18 channels of a circuit in the inset.

Four independent circuits are used to cool the BB, see Figure 5: two for the IB segments and two for the OB segments. Each component of the BMs is cooled in counterflow by the two circuit. The distribution of the helium to the segments is obtained through toroidal manifolds running around the vacuum vessel (Ring Header Distributors and Ring Header Collectors); from each of them, 48 (OB) or 32 (IB) pipes bring the coolant to the segments. The cooling trains, composed by the compressor and heat exchanger (steam generator, SG) are redundant: five trains are used for each of the OB circuits, while two trains cool the IB segments. For each of the four circuits, a spare cooling train is foreseen [14].

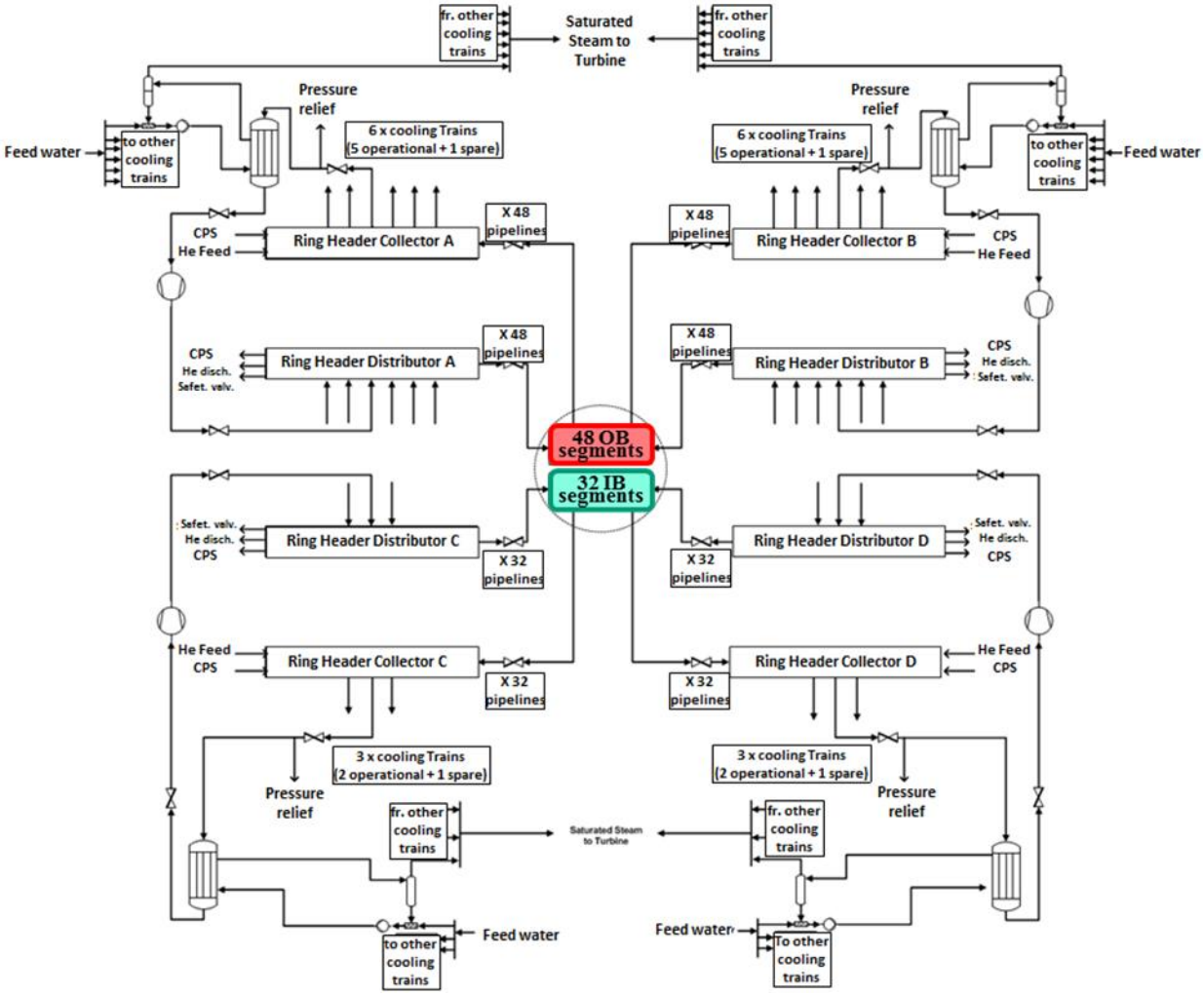

Figure 5: Schematic of the HCPB BB cooling system [14]. A and B refer to the two circuits cooling the OB segments; C and D refer to the two circuits cooling the IB segments.

As far as the distribution of the coolant inside the BMs is concerned, three different options are under investigation: HCPB-I, HCPB-S and HCPB-D [13].

2.1. HCPB-I

The first option, HCPB-I (where the "I" stands for "Integrated"), foresees the series integration of the FW and BZ thermal-hydraulics: in particular, the helium coming from the compressor is initially distributed to the FW channels, then collected and distributed again to the CPs and caps, which are cooled in parallel, see Figure 6. While this configuration allows the direct integration of FW heat loads into the power generation system, it can be applied only if the FW heat flux is reasonably predictable and around 0.5 MW/m², as otherwise the total heat to be removed by the circuit would be too high [13].

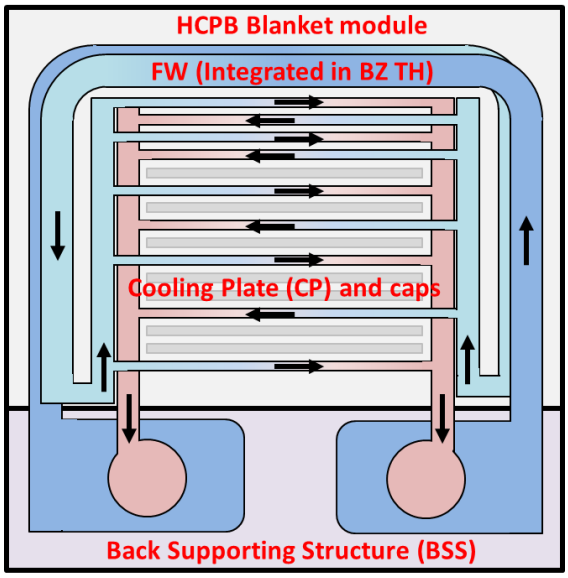

Figure 6: HCPB-I cooling layout [13].

2.2. HCPB-S

In the HCPB-S (where the "S" stands for "Separated") cooling scheme, the FW is cooled by a set of four loops independent from the four used to cool the BZ, see Figure 7; the FW is still part of the BM structure, and its inlet and outlet manifolds are integrated into the BSS. In this case, the FW heat loads cannot be integrated directly in the Primary Heat Transfer System (PHTS), so this solution should be applied only if the FW heat flux is not predictable (but still bounded between 0.3 MW/m² and 1 MW/m²) [13]. Possibly, the FW heat could be used to pre-heat the secondary water before the SG inlet through a dedicated heat exchanger (HX).

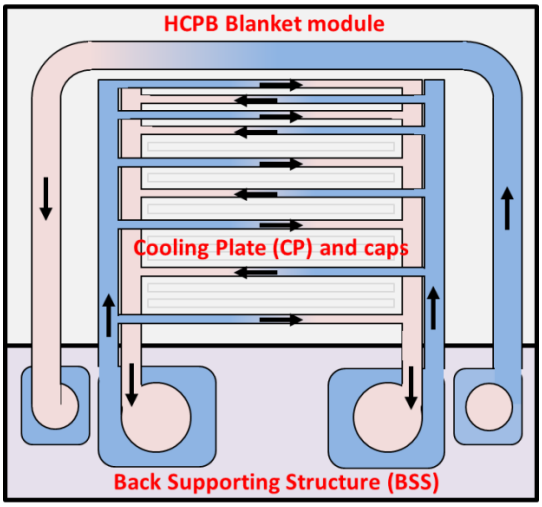

Figure 7: HCPB-S cooling layout [13].

A third option, called HCPB-D (where the "D" stands for "Detached") is foreseen, in which the FW is physically detached from the BM and BSS, allowing a water-cooled FW [13]; since this possibility is beyond the scope of the present work, this scheme has not been considered here. Also, the opportunity to have a mixed approach (with some regions of the blanket in HCPB-I, some in HCPB-S) has not been considered for the time being.

3. Description of the model

In this section a detailed description of the model is given, in terms of equations and modelling approach; then, all the models specifically developed for this work are described, together with their parameterization.

The model is developed with an object-oriented programming (OOP) paradigm, based on the concept of "object": an object is a data structure which can hold variables, functions and other data structures. One of the main advantages of the OOP paradigm is the possibility to simply reuse existing code thanks to the concepts of "extension" and "inheritance": a new object can be defined as an extension of an existing one, inheriting all of its variables and functions, while implementing new characteristics or redefining some of the existing ones.

3.1. Modelling approach and equations

Since the aim of the work is to develop a system-level model, all the circuit components are modelled here with a 0D or 1D (along the fluid flow direction) approach, using a 1D approach if one dimension is prevailing on the others and 0D otherwise. Hence, all the cooling channels are modelled with a 1D Finite Volume (FV) approach, while valves, manifolds and circulators are modelled as 0D objects (the reasons why the manifolds are modelled as 0D objects are explained in the following §3.2.4). The SG is modelled as a perfect HX, i.e. the helium at the HX outlet is always at the nominal temperature (300 °C). The solid structures around the cooling channels are also lumped in a 1D FV model of the channel walls, as explained in the following §3.1.3. Finally, when computing the pressure drop the presence of flow meters or other instrumentation devices is not accounted for.

The model is developed using Modelica, which is an object-oriented, declarative programming language aimed at simplifying the task of the development of models for complex systems [15, 16]. The main reasons behind this choice are exactly in its declarative nature, which allows to develop the model of new objects by simply writing the model equations, and in the extensive experience on it, e.g. for the modelling of the superconducting magnets cooling system [3], developed during the last years at the Energy Department of Politecnico di Torino. Moreover, several libraries for the modelling of energy-related systems are freely available in Modelica. Finally, Modelica was chosen since it will allow adding also other (e.g. electrical) components of the power conversion system to the model in the future, while still being a valid tool for the thermal-hydraulic analyses: in fact, it has already been successfully applied for nuclear fission thermal-hydraulics, showing an excellent agreement when validated against the well-known RELAP code [17].

All the objects for the standard circuit components (valves, circulators, pipes, manifolds), as well as the basic object for the fluid flow modelling, come from the open source *ThermoPower* Modelica library [18, 19].

3.1.1. 1D fluid objects

For the 1D fluid objects (i.e. the cooling channels), the model, extending ThermoPower models, implements the time-dependent mass, momentum and energy conservation equations (1-3) for each fluid volume i (here $\dot{m}_i$ refers to the upstream mass flow rate):

$$\begin{cases} A \cdot l_i \cdot \dfrac{d\rho_i}{dt} = \dot{m}_{in,i} - \dot{m}_{out,i} & (1) \\ \dfrac{l_i}{A} \cdot \dfrac{d\dot{m}_i}{dt} = p_{out,i} - p_{in,i} + \Delta p_{friction,i}\ (+\Delta p_{loc}) & (2) \\ A \cdot l_i \cdot \rho_i \cdot c_{v,i} \cdot \dfrac{dT_i}{dt} + \dot{m}_{out,i} h_{out,i} - \dot{m}_{in,i} h_{in,i} = \dot{Q}_{in,i} & (3) \end{cases}$$

The friction and localized losses are computed with the following equations (4-5):

$$\Delta p_{friction,i} = \frac{2f \cdot l_i \cdot \dot{m}_i^2}{D_h \cdot A^2 \cdot \rho_i} \tag{4}$$

$$\Delta p_{loc} = K \cdot \frac{\dot{m}^2}{\rho} \tag{5}$$

3.1.2. 0D fluid objects

For the 0D fluid objects, the mass and energy balance equations are solved (6-7):

$$\begin{cases} V \cdot \dfrac{d\rho}{dt} = \dot{m}_{in} - \dot{m}_{out} & (6) \\ V \cdot \dfrac{d(\rho e)}{dt} = \dot{m}_{in} h_{in} - \dot{m}_{out} h_{out} + \dot{Q}_{in} & (7) \end{cases}$$

3.1.3. 1D solid objects

For the solid walls, the energy conservation equation is solved, accounting for the heat transfer between solid and fluid, according to equation (8):

$$A_m \cdot \rho_{m,i} \cdot c_{v,i} \cdot \frac{dT_{m,i}}{dt} = \pi D_h \cdot \gamma_i \left(T_{m,i} - T_i\right) \tag{8}$$

3.2. Description of the objects

The structure of the model, considering a single cooling train and showing a single segment, is reported in Figure 8.

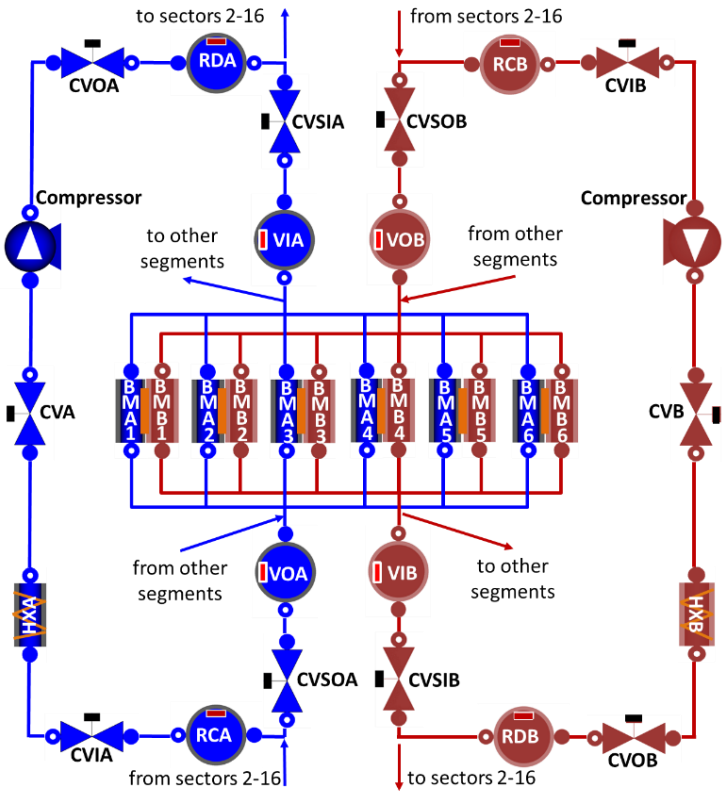

Figure 8: Structure of the HCPB cooling loops model developed in this paper. The twin circuits A and B, see Figure 5 above, are coupled at the BM level (CV: Control Valve; HX: Heat eXchanger; RC: Ring header Collector; RD: Ring header Distributor; V: Volume; BM: Breeding Module; S: Sector; I: Inlet; O:Outlet).

3.2.1. Breeding Module

The basic object of the model is the BM, represented by BMA1-6 and BMB1-6 in Figure 8. The BM object contains one FW object (described in §3.2.2), one BZ object (described in §3.2.3), two BM cap objects (described in §3.2.3) and the inlet/outlet manifold objects (described in §3.2.4).

Different objects have been developed for the HCPB-I and HCPB-S cooling schemes; the former is shown in Figure 9, the latter in Figure 10. In the HCPB-S scheme the BM object contains the BZ and caps only (Figure 10a), while a completely independent object models the two dedicated loops that cool the FW (Figure 10b).

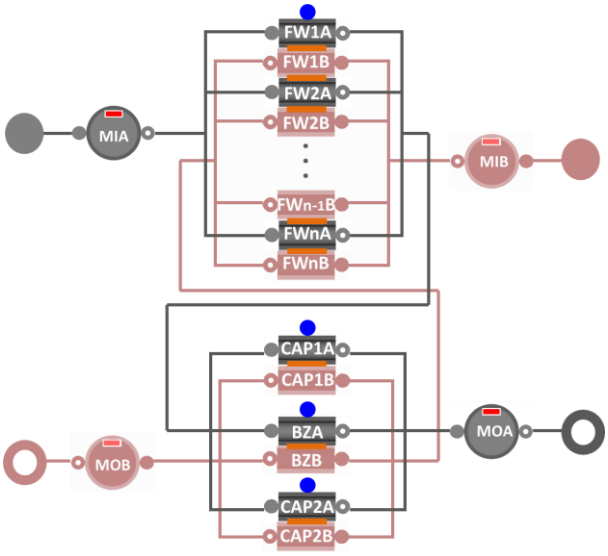

Figure 9: Schematic of the HCPB-I BM object. The blue circles represent the ports for the input power, while the orange rectangles represent the thermal coupling between the counterflow circuits.

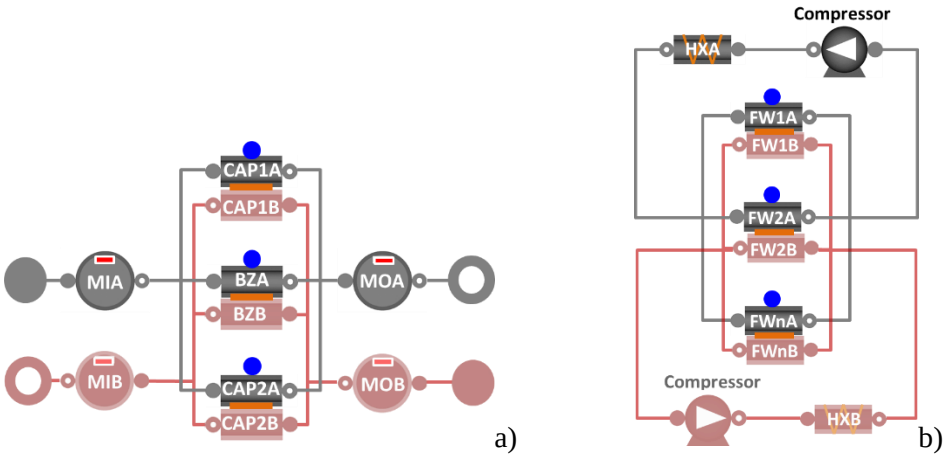

Figure 10: Schematic of the HCPB-S objects: a) BM object for the main loops; object modelling the dedicated loops for FW cooling. The blue circles represent the ports for the input power, while the orange rectangles represent the thermal coupling between the counterflow circuits.

3.2.2. First Wall

A snapshot of the CAD drawing of the OB4 BM FW is shown in Figure 11. The FW object contains several FW channel objects, including connectors for thermal coupling to the neighbouring channels in the twin circuit. A single FW channel object is in turn composed of three channels in series: two channels represent the side parts of the FW, which are heated by the nuclear load and by heat conduction from the BZ; the third channel represents the front part, which is also heated by the plasma surface load on its plasma-facing side. The bends

in the FW channels are accounted for only as 0D localized pressure drops. To ensure the reliability of the developed model, it has been validated against the hydraulic CFD simulations reported in [10].

A schematic of a single FW channel object is shown in Figure 12.

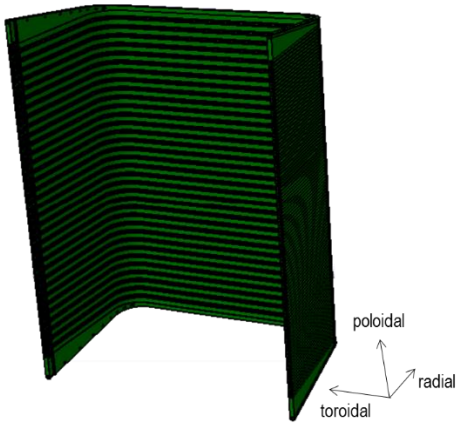

Figure 11: CAD of the OB4 FW.

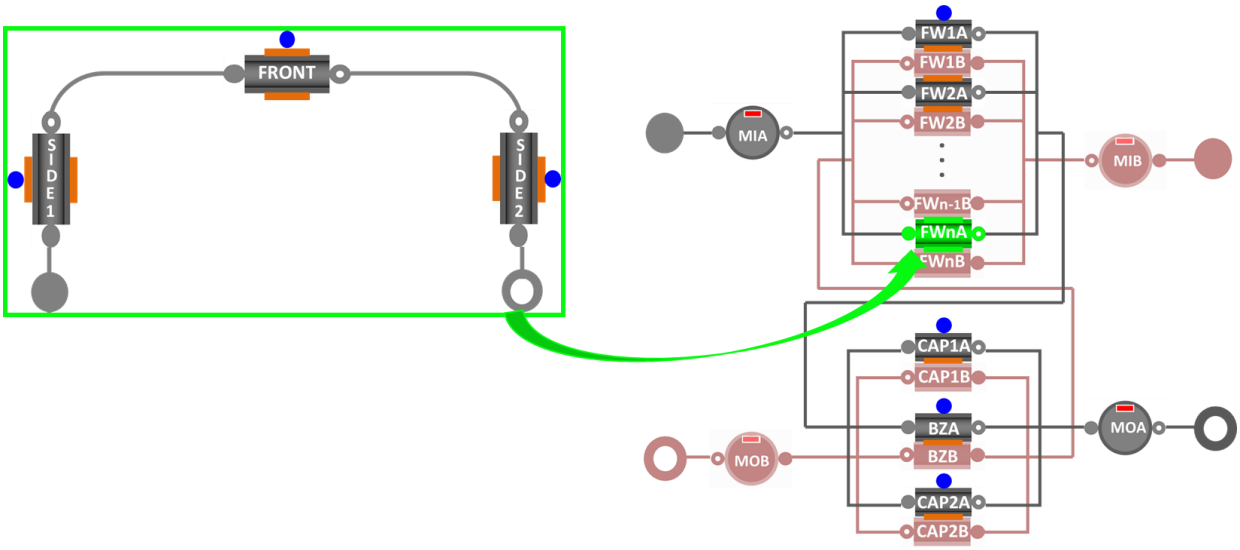

Figure 12: Schematic of a single FW channel object, and its position in the HCPB-I BM object. The orange rectangles (between, e.g., FW1A and FW1B) represent the connectors for the thermal coupling between two neighbouring FW channels, while the blue circles represent the connectors for the input heat loads.

The input parameters that identify the FW objects are:

- Number of FW channels;
- Geometrical data (length, cross section, hydraulic diameter, heated perimeter, wall thickness);
- Thermophysical properties of the coolant (density, viscosity and specific heat capacity), as a function of the thermodynamic state;
- Thermophysical properties of the structural (pipe) material (density, thermal conductivity, specific heat capacity), as a function of the temperature;
- Fanning Friction factor correlations (different for the front and side parts of the channel);
- Localized pressure loss coefficient for the bends.
- Heat transfer coefficient (HTC) correlations (different for the front and side parts of the channel; also, different correlations can be used for the plasma-facing walls and for the non-plasma-facing walls);

- Number of nodes discretizing each of the three parts of a channel.

The geometrical data and the heat loads can be different for each of the FW channels, while all the other parameters are fixed inside each FW object, i.e. are the same for all the FW channels inside a FW object (but can still be different among different FW objects).

3.2.3. Breeding Zone and BM caps

Figure 13 shows a CAD snapshot of the OB4 BM, highlighting the coolant flow path.

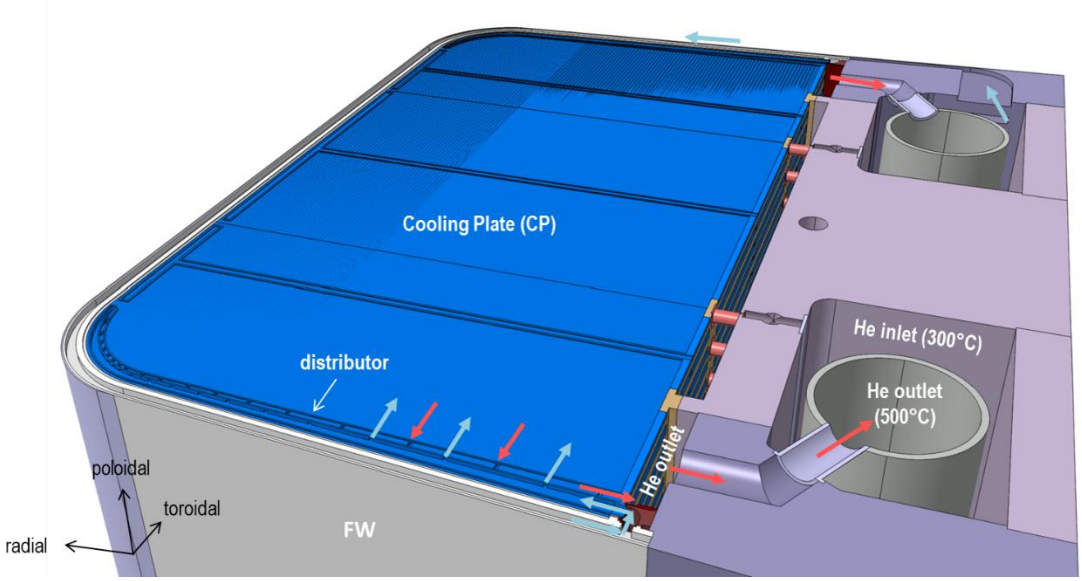

Figure 13: CAD of the OB4 BM, showing the coolant flow path in HCPB-I configuration. Adapted from [13].

Inside the BZ object there are several CP objects (Figure 14a), each of which contains models for the cooling channels (Figure 14b), as well as connectors for inter-channel thermal coupling with the twin circuit (within the same CP). The BM cap object, shown in Figure 14c, is identical to the CP object, but may have a different number of channels; also in this case, connectors to account for thermal coupling between channels in the counterflow circuits are provided. In addition, it is possible to implement orifices at the cap inlet, to better redistribute the mass flow rate among CPs and caps.

Also in this case, the validity of the CP and cap models has been proved by testing them against the hydraulic CFD simulation results available in [10].

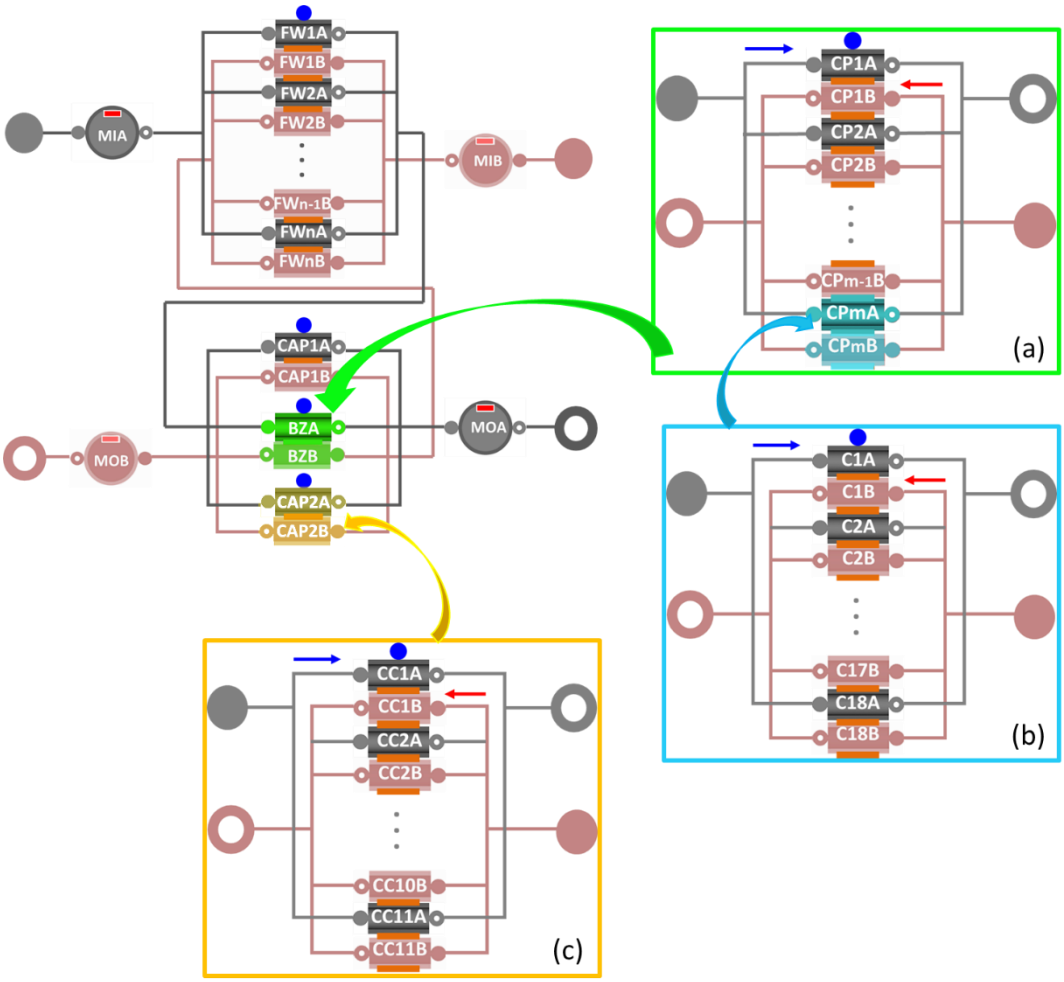

Figure 14: Schematic of the BZ and cap objects and their position in the HCPB-I BM object (top left figure): BZ object containing several CP objects (a); CP object containing several cooling channels ("C" objects) (b); cap object containing several cooling channels ("CC" objects) (c).

The input parameters that identify the BZ and cap objects are:

- Number of CPs (BZ object only);
- Number of channels in each CP/cap;
- Geometrical data (length, cross section, hydraulic diameter, heated perimeter, wall thickness);
- Thermophysical properties of the coolant (density, viscosity and specific heat capacity), as a function of the thermodynamic state;
- Thermophysical properties of the structural material (density, thermal conductivity, specific heat capacity), as a function of the temperature;
- Pressure loss coefficient for the orifice at the cap inlet, see equation (5);
- Fanning Friction factor correlation;
- HTC correlations (different correlations can be used for the plasma-facing walls and for the non-plasma-facing walls);
- Number of nodes discretizing each channel.

As with the FW, the geometrical data and the heat loads can be different for each of the cooling channels in the BZ and caps; the other parameters are fixed for the whole BZ.

3.2.4. BM inlet/outlet manifolds

The coolant flow path in the BM I/O manifolds is visible in Figure 13: the inlet and outlet manifolds for the same loop are coaxial. Although the length of these manifolds is much larger than their transverse dimension, the coolant flow cannot fully develop inside them, because of the distributions of all the inlet and outlet derivations. The consequently complex coolant flow path would call for a 3D CFD modelling of the manifolds, if a detailed computation of pressure drops and coolant distribution should be required; however, this is not currently within the aim of this work, hence a simplified 0D model is used, meaning that no pressure drop nor elevation effects are accounted for in the manifolds and that the coolant is assumed to be uniformly distributed among all the channels and CPs. Moreover, no heat load is considered to be applied on these manifolds, and the heat transfer between inlet and outlet is neglected. Anyway, thanks to the high flexibility of the model, a detailed manifold model, accounting also for 3D pressure drops and elevation effects, could be easily implemented and added to the model, starting from a detailed CFD characterization of these manifolds.

The input parameters of the current 0D model of the manifolds are their volume and the thermophysical properties of the coolant.

3.2.5. Solid structures

The solid structures are modelled as lumped in the 1D walls of the channels. Two walls are attributed to each fluid channel: the solid material between two channels is split in two equal halves, and each of them is associated to one of the walls of the closest fluid channels, as shown in Figure 15 for the case of a CP.

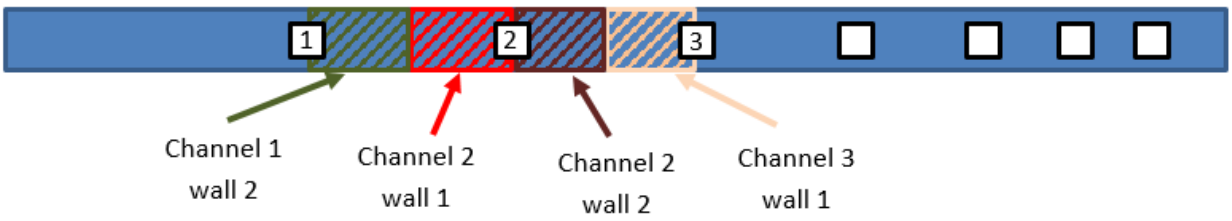

Figure 15: Split of the solid domain between adjacent channels: example related to the unevenly spaced channels of the CPs.

Since the solid parts are dimensionless in the directions perpendicular to the flow path, the temperature of the structure computed by the model has to be considered as an average temperature: the hot-spot temperature cannot be computed directly by a 0D/1D model, but can be obtained in the post-processing phase, adopting an "effective HTC" given by CFD 3D simulations.

4. Simulation setup

In this section the values of the input parameters that have been used for the characterization of the different components in the present work are presented, as well as the heat loads and the boundary conditions (BCs). Since the system is assumed to be fully symmetric in the toroidal direction (both in terms of geometry and heat loads), only one IB segment and one OB segment have been studied, reducing the computational effort.

4.1. Heat loads

Figure 16 shows the baseline heat load for the EU DEMO BB (which is also reported in Table 2), used in the present work, in terms of FW surface load, FW nuclear load and BZ total power generation, respectively. The loads vary with the poloidal position of the BM but are considered uniform inside each BM (i.e., all the loads on the FW are uniformly distributed on the FW channels and all the BZ loads are uniformly distributed among CPs and caps).

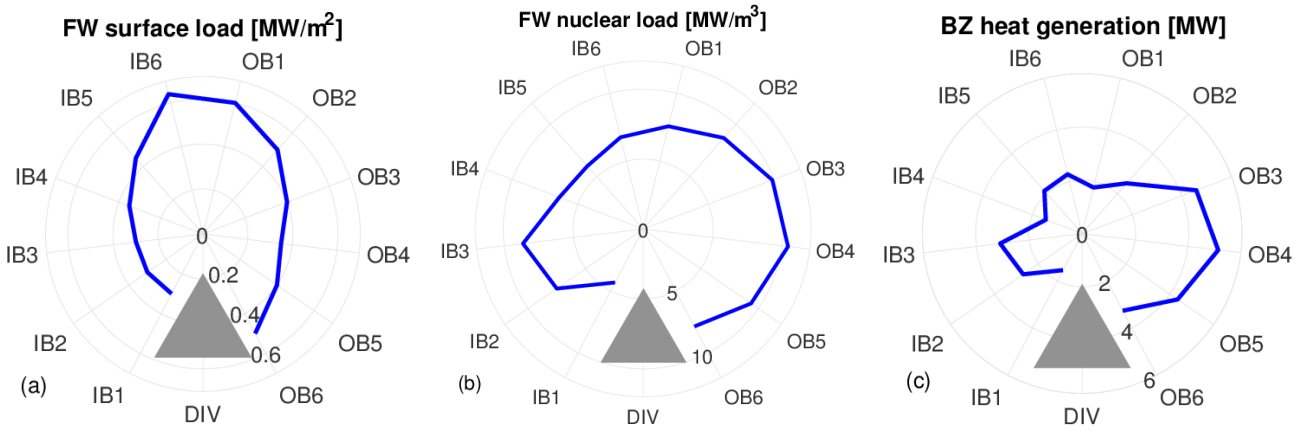

Figure 16: Plot of the poloidal distribution of the heat loads: FW surface load (a), FW volumetric nuclear load (b), BZ heat generation (c) [12]. The triangle represents the divertor (DIV).

Table 2: Poloidal distribution of the heat loads [12].

		BM1	BM2	BM3	BM4	BM5	BM6
FW surface load [MW/m²]	Inboard modules	0.3	0.3	0.3	0.35	0.45	0.64
	Outboard modules	0.6	0.5	0.4	0.35	0.4	0.5
FW volumetric nuclear load [MW/m³]	Inboard modules	4.32	7.50	8.65	6.40	6.01	6.75
	Outboard modules	7.56	8.69	9.87	10.43	9.37	7.87
Heat generated in each BZ [MW]	Inboard modules	1.55	2.69	3.10	1.46	2.14	2.29
	Outboard modules	1.78	2.52	4.58	5.14	4.35	3.27

4.2. Boundary conditions

Although already available in the model, all the ex-vessel components (i.e. compressors, HXs, valves and ex-vessel manifolds) have not been included in the current simulation setup, as the design of these components is at an early stage and no data is available yet about them. Therefore, in order to perform the calculations for the segment, BCs of fixed mass flow rate and fixed outlet pressure (the ideal flow source "m" and pressure sink "p" in Figure 17, respectively) are used, plus a fixed inlet temperature of 300 °C (as the HX is assumed to be ideal, see §3.1). Moreover, in order to simplify the simulation setup and reduce the computational effort, the segment has not been simulated as a whole (i.e., forcing a total mass flow rate through the parallel of the 6 BMs), but each BM has been simulated as a standalone object, forcing an inlet mass flow rate distribution according to the values in [13] and reported in Table 3 (these values have been computed from the enthalpy balance of each BM). The outlet pressure is fixed at 79 bar; since the total pressure drop across the BM in nominal conditions is assumed to be ~1 bar [10], the nominal inlet pressure is 80 bar, but when a higher pressure drop develops, it is free to increase.

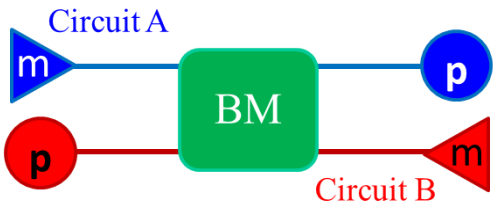

Figure 17: Boundary conditions in the simulation setup used for this work.

Table 3: Mass flow rate forced through the BMs [13].

	BM1	BM2	BM3	BM4	BM5	BM6	**Total**
Inboard modules [kg/s]	5.66	5.24	7.78	5.31	4.99	5.79	**34.8**
Outboard modules [kg/s]	7.87	11.8	14.0	16.8	13.7	10.6	**74.8**

4.3. Input parameters and constitutive relations

4.3.1. First wall

The geometrical data of the first wall used for the present work are reported in Table 4.

Table 4: Geometrical data for the FW.

Length of the side parts [mm]	649.6	
Length of the front part [mm]	1120.5	
Curvature radius of the bending [mm]	156	
Bending angle of the FW [°]	93.75 (IB)	86.25 (OB)
Channel cross section [mm²]	13.5×13.5	
Wall thickness [mm]	2.625 (plasma-facing side)	5.375 (internal side)

To compute the Fanning friction factor for the side parts of the channels, the Blasius correlation [20, p. 490] was used. In the front part the channel is assumed to be ribbed on its plasma-facing wall to improve the heat transfer (Figure 18); the Fanning friction factor correlation

$$f_{ribbed} = 0.1122 \cdot Re^{-0.1854} \tag{9}$$

has been fitted by regression based on the data in [3, 21].

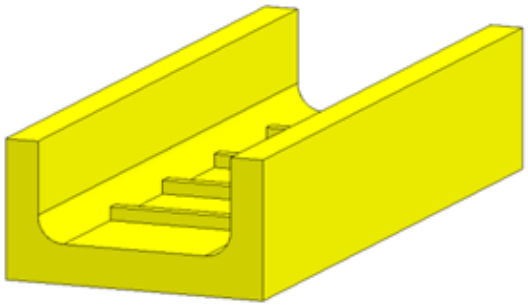

Figure 18: CAD drawing of the ribbed front wall channel [22].

Also for the HTC, two Nusselt number correlations have been obtained by regression on the data in [6, 21, 23]: the first one, valid for smooth FW channels, has been applied to both of the walls of the side parts and to the non-plasma-facing wall of the front part,

$$Nu_{smooth} = 0.334 \cdot Pr^{0.4} \cdot Re^{0.556} \tag{10}$$

The second one, valid for ribbed FW channels, has been applied to the plasma-facing wall of the front part of the channels:

$$Nu_{ribbed} = 0.05533 \cdot Re^{0.749} \tag{11}$$

4.3.2. Breeding zone (CPs), BM caps and manifolds

Tables 5-6 report the geometrical data for the CPs, BM caps and manifolds, as used in the present work; all the CPs are composed of 36 cooling channels (18 per loop), while the caps have 22 channels (11 per loop). The Colebrook correlation [24, p. 429] was used for the friction factor, while the Gnielinski correlation [20, p. 515] was chosen for the HTC.

Table 5: Geometrical data for the CP and cap channels.

	CP	Cap
Length [mm]	1506 (first) ÷ 1132 (last)	1516 (first) ÷ 1120 (last)
Cross section [mm²]	5×2.5	13.5×6
Poloidal wall thickness [mm]	1	10
Radial wall thickness [mm]	29.2 (first) ÷ 3.5 (last)	38 (first) ÷ 2 (last)

Table 6: Volumes of the manifolds.

Inlet [m³]	0.171
Outlet [m³]	0.0713

4.3.3. Numerics

A grid independence study was performed to choose a suitable number of nodes for all the channels, trying to reduce as much as possible the computational cost. For the present work, 15 nodes have been used for the FW channels, while 10 nodes are used for the BZ and caps cooling channels.

5. Results

Two scenarios have been considered in the simulations. In the first one (Scenario A), a steady-state situation is considered, with a constant load reported in Table 2: the model is used there to compare the HCPB-I and HCPB-S designs, and to suggest possible improvements in the cooling system. In the second one (Scenario B), the dynamic capabilities of the model are tested, applying a pulsed load to the OB4 BM in HCPB-I configuration, according to the pulse profile shown in Figure 19 (2 h of plasma followed by 40' of dwell time), for 9 consecutive pulses (i.e., 24 h of operation).

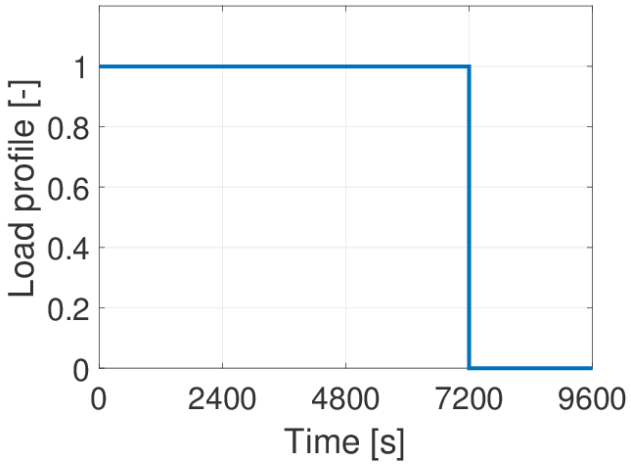

Figure 19: Heat load waveform applied to the BM in the Scenario B (only one period out of 9 is shown).

As explained above, all the FW channels are subject to the same load and have the same properties, as the coolant is assumed to be uniformly distributed among the channels (see §3.2.4), so that the mass flow rate in each FW channel is just the value in Table 3 divided by the number of channels reported in Table 1 (e.g.,

considering OB4, all the FW channels see 115 g/s of coolant, given as 16.8 kg/s / 112 channels). Because of these assumptions, all the channels exhibit exactly the same behaviour, and the reported results, in terms of pressure drop and temperature distribution refer just to one of them. The same consideration applies to the BZ object, as all the CPs are identical and the different length of the channels inside a CP has a negligible bearing on the results (always below 1%). Actually, also some edge effects are present, due to the fact that the first and last channels are coupled with only one channel; these effects are correctly accounted for by the model, but, since the resulting deviation of the results was always found to be lower than 5‰, the reported results refer to channels in the "bulk" without losing generality. Moreover, the two counterflow loops are perfectly antisymmetric, so we report the temperature and pressure drop distributions for only one of them.

As a consequence of the forced mass flow rate distribution explained in §4.2, the pressure drops can be different among the BMs, even though they are supposed to be cooled in parallel; this implies that, if this is the wanted mass flow rate distribution, orifices shall be added in the circuit in series with the BMs showing a lower pressure drop.

Finally, considering that the design of the HCPB cooling layout is still ongoing, the presented results have the objective of showing how this model might be used to optimize the coolant distribution, and should not be taken as "final" results, as they are obtained *before any optimization is applied*.

5.1. Scenario A – Steady state comparison between HCPB-I and HCPB-S configurations

5.1.1. HCPB-I

The distribution of the pressure drops among the different parts of the cooling loop of each BM in the IB and OB segments is reported in Table 7. The pressure drop in the FW region results always ~1 order of magnitude higher than that in the BZ, as expected: in fact, the FW channels are longer and ribbed in their front part; in addition, since the total number of FW channels is much lower than the total number of CP channels, the mass flow rate in each of the FW channels is higher than that in each CP channel. The effect of the ribs in the FW channels is also shown in Figure 20, where the distribution of the pressure drop inside the FW channels is reported: while the front part is ~2× longer than the side parts, the pressure drop is always ~6× bigger (the mass flow rate is of course the same since the two side parts and the front part are in hydraulic series, see Figure 12a). The pressure drop in the non-ribbed side parts is comparable in absolute value with that of the BZ region, even if the channels are ~2× shorter, because of the higher mass flow rate. Because of symmetry, the inlet and outlet side have almost the same pressure drops, with small differences due to the change in the coolant density and viscosity with the temperature.

Even if all the BMs share the same geometry and friction factor correlation, some differences are found among them. These are driven by the different values of mass flow rate forced through the whole BM, the different number of channels and the different heat loads. In fact, the two BMs showing the largest pressure drop among the IB BMs are the IB3 and the IB6: the former one has the highest total mass flow rate and BZ heat load, while the latter has the highest FW heat load and the lowest number of channels and CPs (so that the mass flow rate per channel is almost the same for IB3 and IB6). IB1 and IB2, instead, have the largest number of channels and CPs, and consequently show the lowest pressure drops. Among the OB BMs, instead, the pressure drop distribution is mainly driven by the total mass flow rate: in fact, the BMs with the largest pressure drop are the OB3-5, which are also the ones with the largest flow rate, see Table 3.

Finally, the pressure drop in all the OB BMs is ~3× larger than that in the respective IB BM; this effect, however, is only due to the larger mass flow rate that is forced through the OB BMs.

Table 7: HCPB-I. Pressure drop across the BMs.

Inboard			Outboard		
	Region	Pressure drop [bar]		Region	Pressure drop [bar]
IB1	FW	0.477	OB1	FW	1.00
	BZ	0.0517		BZ	0.0853
	Total	0.529		Total	1.09
IB2	FW	0.421	OB2	FW	1.74
	BZ	0.0488		BZ	0.145
	Total	0.470		Total	1.88
IB3	FW	0.856	OB3	FW	2.33
	BZ	0.0694		BZ	0.118
	Total	0.925		Total	2.45
IB4	FW	0.617	OB4	FW	2.90
	BZ	0.0544		BZ	0.220
	Total	0.672		Total	3.12
IB5	FW	0.624	OB5	FW	2.03
	BZ	0.0558		BZ	0.155
	Total	0.680		Total	2.18
IB6	FW	0.823	OB6	FW	1.31
	BZ	0.0732		BZ	0.0675
	Total	0.896		Total	1.38

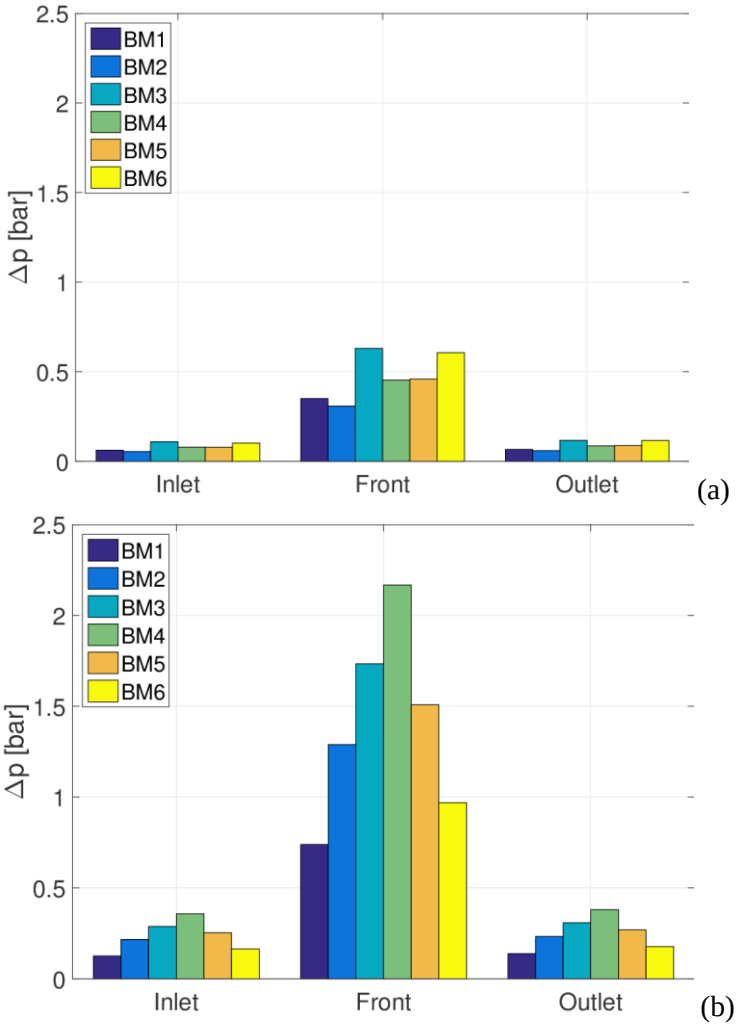

Figure 20: HCPB-I. Share of the pressure drop among the three parts of the FW channels: IB BMs (a) and OB BMs (b).

Figure 21 shows the temperature distribution along the helium flow path for all the BMs. The peak temperature, reached of course in the BZ region, overcomes the safety limit (supposed to be at 500 °C, to keep the structures below 550 °C), because of the uneven distribution of mass flow rate among CPs and caps explained below. Some of the curves are not monotonically increasing in the BZ region and the temperature decreases close to the outlet; this is because the last fluid volumes are coupled with the first fluid volumes (close to the inlet) in the counterflow circuit, where the temperature is lower, and thus the heat transferred to the coupled circuit is higher than the heat load in those nodes. This, however, does not necessarily happen for all the BMs, because of the differences in the mass flow rate (which affects the HTC between the two loops, as well as the cooling of the single channel) and in the heat loads, which may lead to smaller temperature differences between the two neighbouring channels, reducing the heat transfer between them. The temperature in the FW is considerably lower, and the largest temperature increase in this region occurs in the front part, because of the higher load. Also the caps, even if they have the same load as a single CP, reach a much lower peak temperature. This can be explained by looking at how the mass flow rate splits between CPs and caps, shown in Figure 22: in fact, the channels in the caps are in lower number, and have a larger cross section, thus reducing the friction. Consequently, even if the caps represent 2% to 5% of the total number of plates in the BM, they account for 20% to 30% of the total mass flow rate; hence, the cooling of the CPs is less effective and the temperature increase is much higher. A simple way to reduce the maximum helium temperature is to introduce orifices at caps inlet, to increase the overall pressure drop in the caps and mitigate this mass flow rate unbalance, such that the mass flow rate inside is CP is similar to that inside each cap.

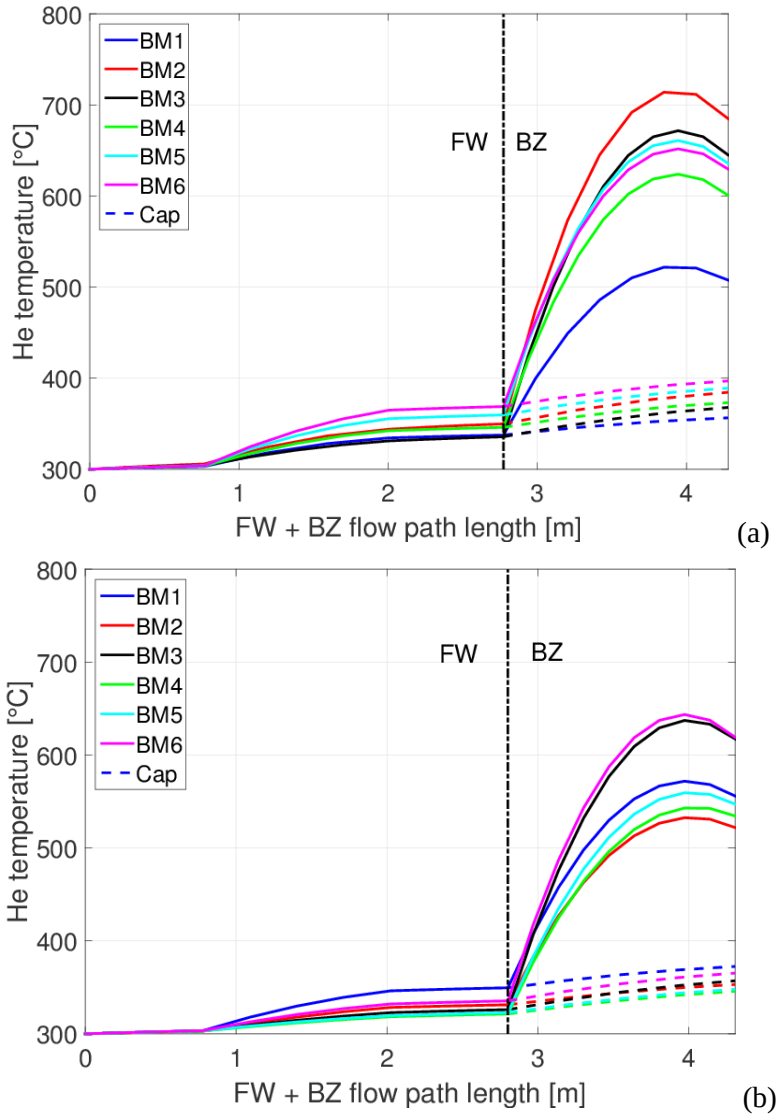

Figure 21: HCPB-I. Temperature distribution in the 12 BMs: IB BMs (a) and OB BMs (b). The dashed lines in the BZ region refer to the caps.

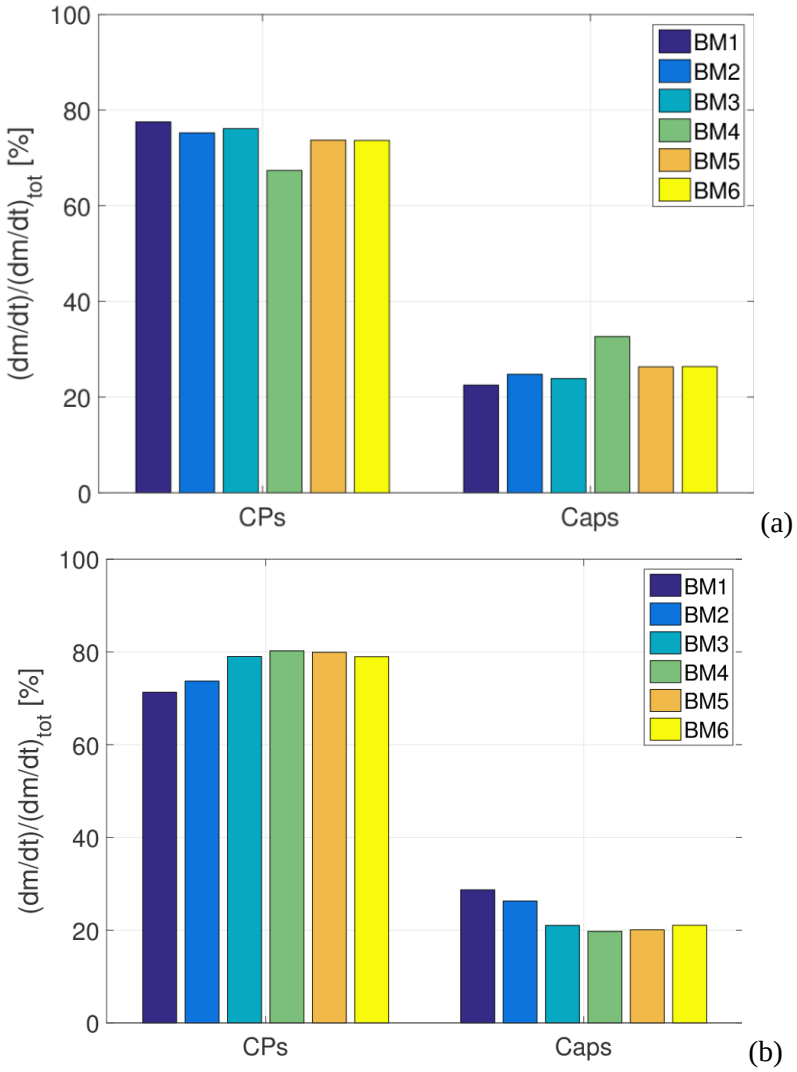

Figure 22: HCPB-I. Share of the mass flow rate among CPs and caps: IB BMs (a) and OB BMs (b).

The implementation of orifices at the caps inlet highly improves the cooling of the CPs, and the temperature reduction is such that the total mass flow rate can even be halved without affecting the cooling performances: Figure 23 shows the temperature distribution in the BM cooling path when orifices are implemented at cap inlet and the mass flow rate forced through the BM is half of that reported in Table 3. The peak temperature is now below the safety limit, with the exception of some IB BMs (where the peak temperature is indeed lower than before), and this has been achieved with a strong reduction of the mass flow rate; also, the temperature increase is similar between caps and CPs, as expected since they have the same load. This is because, as shown in Figure 24, the introduction of the orifices distributes more homogeneously the mass flow rate among CPs and caps, ensuring efficient cooling of both.

Finally, since it is now possible to reduce the mass flow rate without degrading the heat removal efficiency of the system, the total pressure drop across the BM is reduced by a factor of ~2, even if an orifice has been added. Considering that the power required by the circulator is proportional to the product of pressure drop and mass flow rate, it is reduced by a factor of ~4.

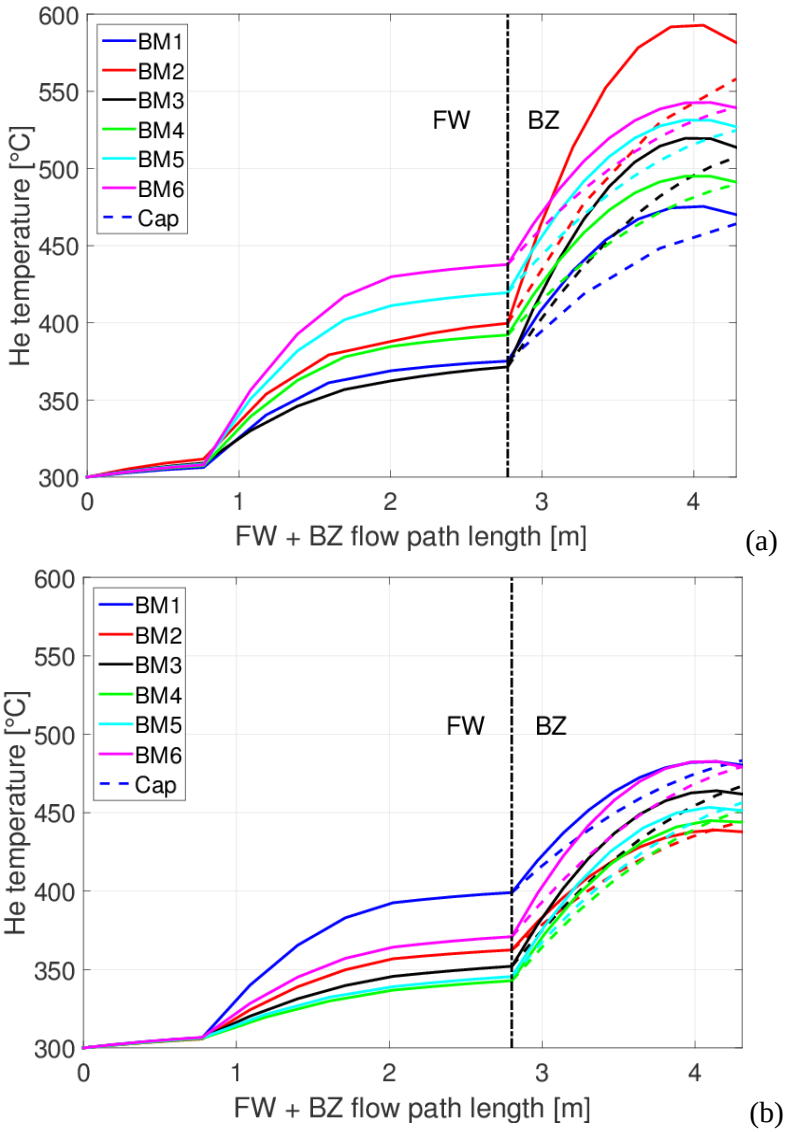

Figure 23: HCPB-I. Temperature distribution in the 12 BMs, when orifices are introduced at the cap inlets: IB BMs (a) and OB BMs (b). The dashed lines in the BZ region refer to the caps.

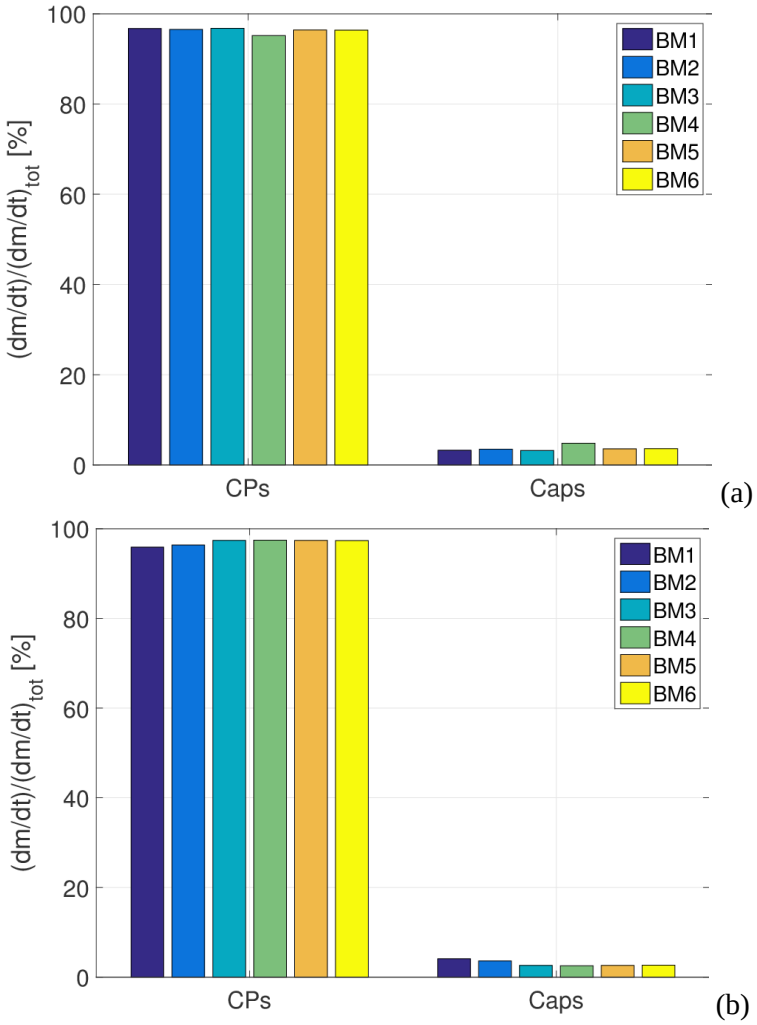

Figure 24: HCPB-I. Share of the mass flow rate between CPs and caps, when orifices are introduced at the cap inlets: IB BMs (a) and OB BMs (b).

5.1.2. HCPB-S

Considering what has been found for the HCPB-I, the simulations performed in the HCPB-S configuration have been carried out with the orifice at the caps inlet. For both the FW cooling loops and the BZ cooling loops, the forced mass flow rate is then half of the values reported in Table 3.

Since the inlet conditions are identical, the results for the FW loop are very close to those found for the HCPB-I configuration when the mass flow rate was halved: in fact, as it is visible in Table 8, the pressure drop in the FW region is ~1/4 of that found in Table 7, as $\Delta p \propto \dot{m}^2$. In addition, for the BZ the results are close to those found for the HCPB-I configuration with the orifice at cap inlet (with a small difference due to the different inlet conditions); the effect of the orifice is to increase the pressure drop in the BZ of ~3×, making its value comparable to that of the FW.

Also in this case, the BMs showing the largest pressure drops are those with the largest mass flow rate and/or the highest loads, and the differences between IB and OB are only driven by the different mass flow rate.

Table 8: HCPB-S. Pressure drop across the 6 IB BMs.

Inboard			Outboard		
	Region	Pressure drop [bar]		Region	Pressure drop [bar]
IB1	FW	0.145	OB1	FW	0.309
	BZ	0.131		BZ	0.305
IB2	FW	0.131	OB2	FW	0.520
	BZ	0.127		BZ	0.545
IB3	FW	0.258	OB3	FW	0.691
	BZ	0.197		BZ	0.448
IB4	FW	0.190	OB4	FW	0.857
	BZ	0.194		BZ	0.626
IB5	FW	0.196	OB5	FW	0.599
	BZ	0.194		BZ	0.439
IB6	FW	0.261	OB6	FW	0.394
	BZ	0.253		BZ	0.247

Figures 25-26 show the temperature distribution in the FW and BZ, respectively. The temperature evolution in the FW is almost unaffected by the different configuration, as the inlet conditions are always the same; the shape of the temperature distribution is the same also in the BZ region, but, since the inlet temperature is lower, the peak temperature stays always below the safety limit also for those IB BMs that overcame it with HCPB-I. This could suggest the use of HCPB-S only in those BMs where the FW load overcomes the HCPB-I limit of 0.5 MW/m² (see §2.1), so that the FW can be directly integrated in the primary loop when possible but keeping the structures in the safe temperature range. For the OB BMs, instead, it is now clear how the modules having the highest load in the BZ region are the least loaded in the FW region: this favourable condition allows using the HCPB-I in the whole OB segment. In fact, as it was shown in Figure 23b, even with that configuration the temperature never exceeded the safety limit.

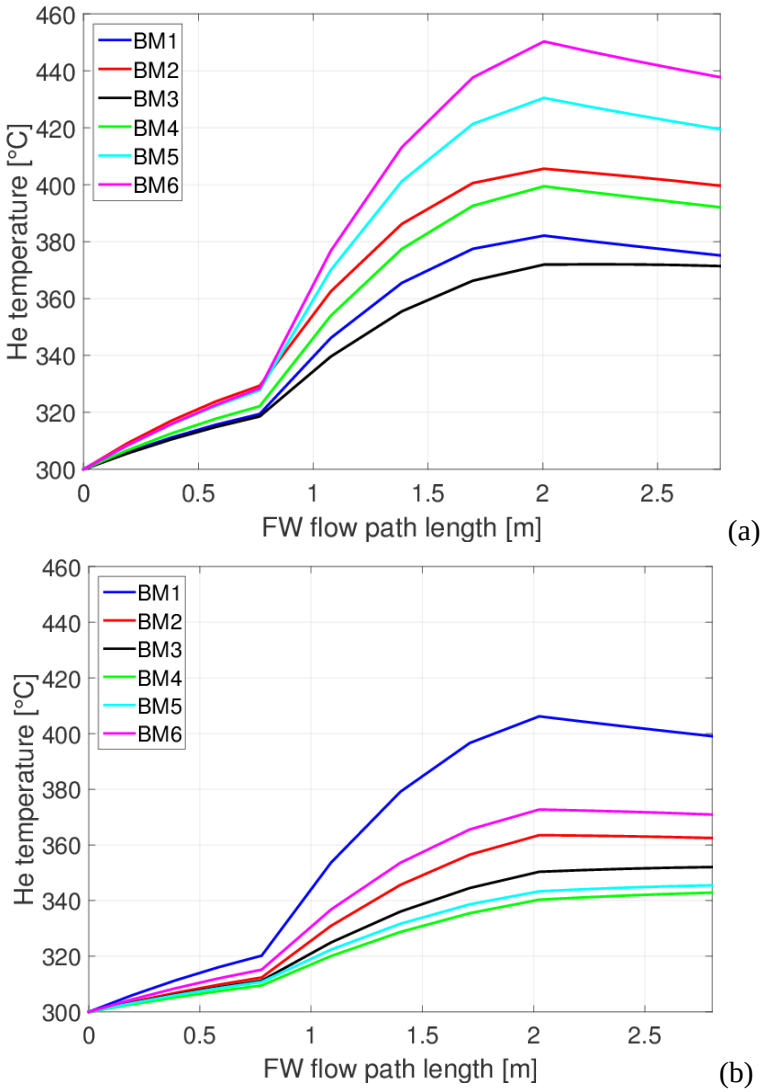

Figure 25: HCPB-S. Temperature distribution in the FW channels of the 12 BMs: IB BMs (a) and OB BMs (b).

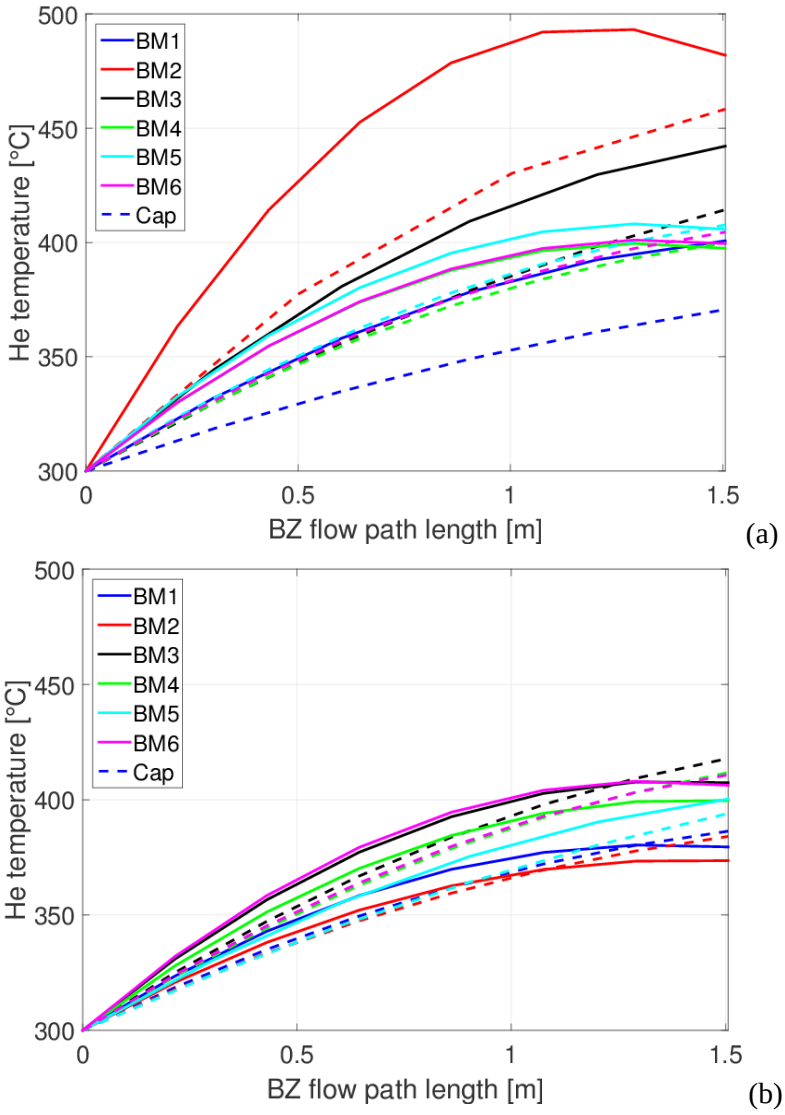

Figure 26: HCPB-S. Temperature distribution in the BZs of the 12 BMs: IB BMs (a) and OB BMs (b). The dashed lines refer to the caps.

5.2. Scenario B – Pulsed operation in HCPB-I configuration

Figure 27 shows the evolution of the maximum coolant temperature reached in the three regions (FW, CPs and caps) of the equatorial OB4 BM in HCPB-I configuration, while Figure 28 shows the evolution of the pressure drop across the different components of the BM. As explained at the beginning of §5, also in this transient simulation the effects of the different length of the CP channels closer to the plasma, as well as edge effects, do not affect significantly the outcome, so only one temperature evolution per region is shown.

The time constant of the transient is much smaller than the duration of the two pulse phases (plasma burn, 7200 s and dwell time, 1400 s, see Figure 19), as found also in [25], so the temperature and the pressure drop rapidly reach a plateau (at the same values shown in the Scenario A steady-state analysis) and stay constant for most of the time.

Also, the dwell time is long enough for the temperature to go back to 300 °C across the whole BM, and for the pressure drop to go back to the initial value, so periodic behaviour is reached already after a single pulse, i.e. each pulse starts from the same initial conditions and all the pulses are perfectly equal (hence, only one is shown).

While the maximum temperature is reached at the outlet of the BZ region, with similar values for CPs and caps (thanks to the implementation of orifices as explained in §5.1.1), the most notable difference is in the different slope of the temperature variation between CPs and caps, with the caps showing a slightly slower response, visible in Figure 27. This effect can be explained by the different cooling configuration of a CP and a cap: the orifice has in fact been optimized in order to have the same total mass flow rate in a cap and in a CP, but while the total flow cross section in a cap is 891 mm², that of a CP is only 225 mm², which is ~¼; since $\dot{m} = \rho A v$, the velocity inside a cap channel is ~¼ of that inside a CP channel, so the heat advection is slower in the caps. This effect is partially compensated by the different masses of the channel walls for a CP and a cap: in fact, since the total flow area in a cap is larger than that for a CP, the total solid mass in a CP is larger, increasing the thermal inertia of a CP. The combined effect of these two phenomena is that the transient in the caps is slower by a factor of ~2.

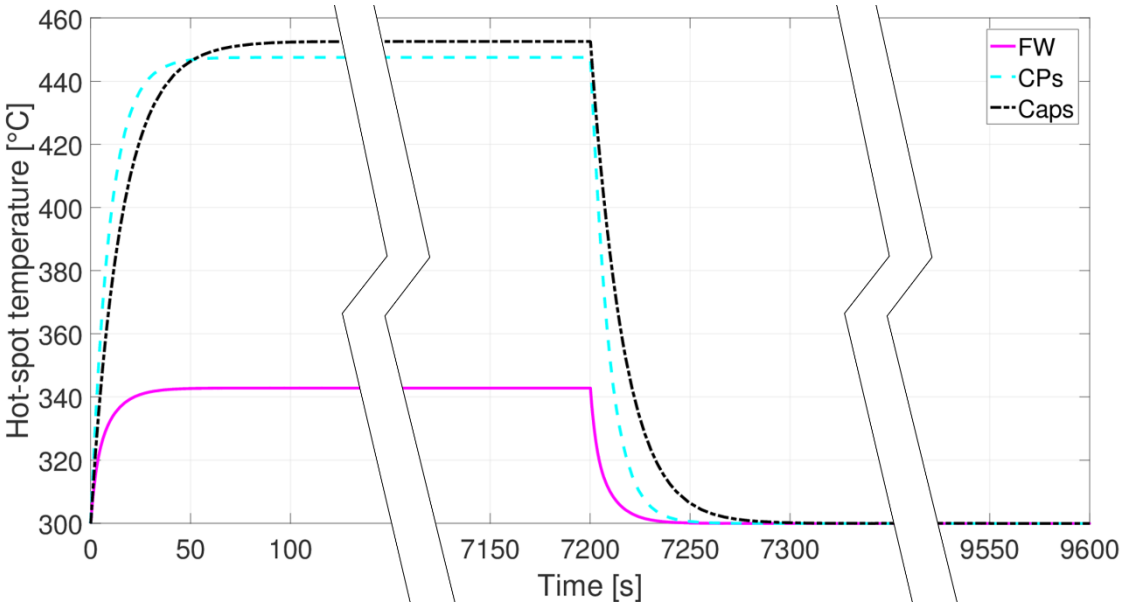

Figure 27: HCPB-I. Evolution of the hot-spot temperature in the OB4 BM during a plasma pulse: FW (solid line), CPs (dashed line), caps (dash-dotted line).

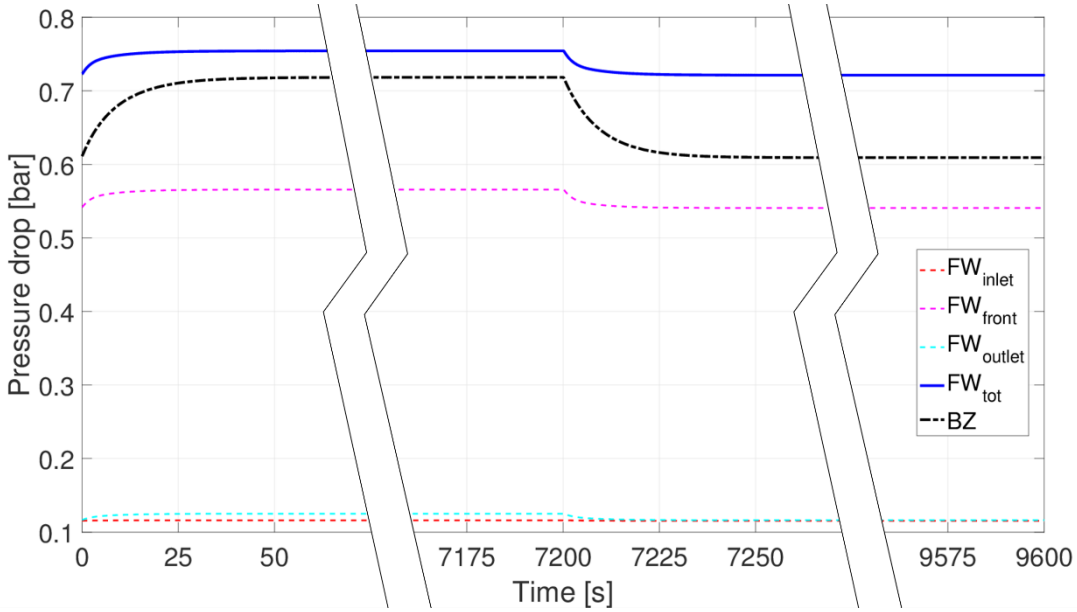

Figure 28: HCPB-I. Evolution of the pressure drop in the OB4 BM during a plasma pulse: FW (solid line) and BZ (dash-dotted line); also the distribution of the pressure drop among the three parts of the FW channels is shown (dashed lines).

6. Conclusions and perspective

A model for the EU DEMO HCPB BB cooling loops has been developed, which allows the transient simulation of the coupled helium cooling loops according to the 2014 design. The model, written using the object-oriented Modelica language, is fully modular and allows comparing different scenarios or cooling scheme configurations, and can be easily adapted to future BB designs.

The model has been tested against two different scenarios: first, it has been used to perform a comparison of the steady-state performance of two cooling schemes, the first one with the FW fully integrated in the BZ cooling loop (HCPB-I), the other one with a fully decoupled FW (HCPB-S). The model helped identifying the most critical BMs, where HCPB-I might not be applicable and HCPB-S should be used. Moreover, the model showed the unbalance among CP and caps cooling, and suggested that implementation of orifices at specific locations along the cooling path can improve the thermal-hydraulic performance of the system, while simultaneously reducing the pumping power, as it allows a reduction of the mass flow rate.

Secondly, the dynamic capabilities of the model have been proved by simulating one BM during a pulsed operation scenario. This analysis confirmed that the transients in the BB cooling loops are much faster than the characteristic times of the EU DEMO pulsed operation, so that steady-state conditions are quickly reached during the pulse.

The model is being extended to the case of the Water-Cooled Lithium Lead (WCLL) BB concept, currently under development. In the future, these two models might also be compared and validated against well-established nuclear thermal-hydraulic codes, such as RELAP, in order to further confirm their reliability for the EU DEMO design and analysis.

Acknowledgements

This work has been carried out within the framework of the EUROfusion Consortium and has received funding from the Euratom research and training programme 2014-2018 under grant agreement No 633053. The views and opinions expressed herein do not necessarily reflect those of the European Commission.

The authors wish to thank Dr. Gianfranco Federici for his appreciated support to this work, Dr. Lorenzo Boccaccini and Dr. Francisco Hernández for providing input and helpful hints on the HCPB design. Finally, the authors wish to thank also Dr. Frederik Arbeiter for a critical reading of the manuscript, leading to many improvements.

References

[1] F. Romanelli, P. Barabaschi, D. Borba, G. Federici, L. Horton, R. Neu, D. Stork and H. Zohm, "Fusion Electricity – A roadmap to the realisation of fusion energy," European Fusion Development Agreement (EFDA), 2012.

[2] O. Costa Garrido, B. Končar, S. Košmrlj, C. Bachmann and B. Meszaros, "Global thermal analysis of DEMO Tokamak," in *24th International Conference Nuclear Energy for New Europe*, Portorož, Slovenia, September 14-17, 2015.

[3] F. Arbeiter, C. Bachmann, Y. Chen, M. Ilić, G. Schlindwein, F. Schwab, B. Sieglin and R. Wenninger, "Thermal-hydraulics of helium cooled First Wall channels and scoping investigations on performance improvement by application of ribs and mixing devices," *Fusion Engineering and Design (http://dx.doi.org/10.1016/j.fusengdes.2016.01.008),* 2016.

[4] L. V. Boccaccini, R. Meyder and J. X., "Analysis of three LOCAs for the European HCPB test blanket system," *Fusion Engineering and Design,* vol. 82, no. 15-24, pp. 2335-2340, 2007.

[5] M.-Y. Ahn, S. Cho, D. Y. Ku, H.-S. Kim e J.-S. Suh, «LOCA analysis for Korean helium cooled solid breeder TBM,» *Fusion Engineering and Design,* vol. 84, n. 2-6, pp. 380-384, 2009.

[6] J. Wang, W. Tian, G. Su, Q. Suizheng, B. Xiang, G. Zhang e K. Feng, «Thermal–hydraulic and safety analysis for Chinese helium-cooled solid breeder TBM cooling system,» *Fusion Engineering and Design,* vol. 88, n. 1, pp. 33-41, 2013.

[7] L. Savoldi Richard, F. Casella, B. Fiori e R. Zanino, «The 4C Code for the Cryogenic Circuit Conductor and Coil modeling in ITER,» *Cryogenics,* vol. 50, pp. 167-176, 2010.

[8] R. Zanino, R. Bonifetto, F. Cau, A. Portone and L. Savoldi Richard, "CFD Analysis of the ITER First Wall 06 Panel. Part II: Thermal-Hydraulics," *Fusion Engineering and Design,* vol. 89, pp. 431-441, 2014.

[9] L. Savoldi Richard, R. Bonifetto, R. Zanino, S. Corpino, G. Obiols-Rabasa, J. Izquierdo, R. Le Barbier e Y. Utin, «CtFD Analysis of a Regular Sector of the ITER Vacuum Vessel. Part I: Flow Distribution and Pressure Drop,» *Fusion Engineering and Design,* vol. 88, pp. 3272-3279, 2013.

[10] P. Norajitra, M. Oron-Carl, O. Bitz, V. Chakin, D. Demange, M. Genzalez, F. Hernandez, T. Hernandez, U. Fischer, Q. Kang, B. Kiss, R. Knitter, H. Neuberger, P. Pereslavtsev, G. Porempovics and P. Vladimirov, "DDD 2014 for HCPB," EFDA_D_2MCQCX v1.1, 2015.

[11] L. V. Boccaccini, "EU blanket design and R&D for DEMO," 2nd EU-US DCLL Workshop, UCLA, 14-15 November 2014. [Online]. Available: http://www.fusion.ucla.edu/FNST/EU-US_DCLL-14-15-Nov-2014/Presentations/Friday/Boccaccini-DCLL_Workshop_presentation_v2-0.pdf. [Accessed 26 April 2016].

[12] C. Bachmann, "Development of a system level thermohydraulic model of the DEMO tokamak," EFDA_D_2MBW7Q, 2015.

[13] F. A. Hernández Gonzalez, "Thermo-hydraulic layout of the HCPB segment," 1st BB Design Progress Review Meeting, Garching, June 23, 2015.

[14] P. Norajitra and D. Carloni, “Summary of key parameters for the design of the PHTS and related BoP for the HCPB,” EFDA_D_2MBDM2 v1.1, 2014.

[15] S. Mattsson, H. Elmqvist and M. Otter, “Physical systems modeling with Modelica,” *Control Engineering Practice,* vol. 6, pp. 501-510, 1998.

[16] P. Fritzson, Principles of object-oriented modeling and simulation with Modelica 2.2, Wiley, 2003.

[17] A. Cammi, F. Casella, M. E. Ricotti e F. Schiavo, «An object-oriented approach to simulation of IRIS dynamic response,» *Progress in Nuclear Energy,* vol. 53, n. 1, pp. 48-58, 2011.

[18] F. Casella and A. Leva, “Modelica open library for power plant simulation: design and experimental validation,” *Proceedings of 3rd International Modelica Conference,* pp. 41-50, Linköping, Sweden, 3-4 November 2003.

[19] F. Casella and A. Leva, “Modelling of thermo-hydraulic power generation processes using Modelica,” *Mathematical and Computer Modelling of Dynamical Systems,* vol. 12, no. 1, pp. 19-33, 2006.

[20] F. Incropera and D. Dewitt, Fundamentals of heat and mass transfer, 6th edition: John Wiley & Sons, 2006.

[21] S. Ruck and F. Arbeiter, “Thermohydraulics of Rib-Roughened Helium Gas Running Cooling Channels for First Wall Applications,” *Fusion Engineering and Design (http://dx.doi.org/10.1016/j.fusengdes.2016.01.029),* 2016.

[22] F. Arbeiter, T. Böttcher, Y. Chen, M. Ílic, Q. Kang, C. Klein, P. Moster and F. Schwab, “Helium-cooled First Wall optimization study,” EFDA_D_2MJ97F v1.2, 2014.

[23] F. Arbeiter, *Personal communication.*

[24] B. R. Munson, T. H. Okiishi, W. W. Huebsch and A. P. Rothmayer, Fluid Mechanics, John Wiley and Sons, 2013.

[25] T. N. Todd, R. Clarke, H. Kalsi, M. Kovari, A. Martin, A. Muir and Z. Vizvary, “The key impacts of pulsed operation on the engineering of DEMO,” EURATOM-CCFE Fusion Association, Culham Science Centre, Abingdon, Oxfordshire OX14 3DB, 2010.